# ENHANCING THE STAB RESISTANCE OF FLEXIBLE BODY ARMOR USING FUNCTIONALIZED $SIO_2$ NANOPARTICLES

**Floria E. Clements*, Hassan Mahfuz**
*** Florida Atlantic University, Department of Ocean Engineering – Nanocomposites Laboratory, Boca Raton, Florida USA**

***Abstract***

*Nanoscale silica particles are functionalized and ultrasonically dispersed into a mixture of polyethylene glycol and ethanol, and then reinforced with Kevlar. The stab or puncture resistance of the flexible nanophased materials system supersedes recent advances made in this area. Through SEM scans, thermal and chemical analysis, it is evident that the functionalized nanoparticles offer multiple facets of resistance to penetration of a sharp impactor. The improvement in protection is traced to the formation of siloxane bonds during functionalization. The framework for a theoretical model is established to estimate penetration depth under low velocity impact of a sharp object through the flexible composite.*

## 1 Introduction

Development of body armor for soldiers has been aimed towards ballistic protection. Because ballistic protection mainly consists of rigid panels (i.e. ceramic plates) inserted into a fabric pouch or incorporated in hard formed gear, it is restricted to the head and torso and does not include the extremities such as hands, arms, necks, and legs. The head and torso are extremely important to protect because these areas consist of life supporting organs. Due to increased casualties as a result of extremity injuries and the increase in soldiers' carryon loads, much development in lightweight and flexible warrior systems has been explored. The need for lightweight and flexible armor is to maximize maneuverability without sacrificing protection of the soldier. In addition to ballistic resistance, attention is given to threats imposed by sharp weapons rather than by guns. The flexible armor that has been developed usually gives resistance against ballistics only or sharp cutting impacts only. Protection against both threat systems incorporating the desired lightweight and flexible characteristics is under continual investigation.

Deshmukh and McKinley [1] studied liquid infused fabric body armor which resists impact when under a magnetic field. This material is called magnetorheological (MR) fluid which consists of iron particles. Works by Gadow *et al.* [2] studied the stab resistance of a thermally sprayed ceramic and cermet coatings on aramid fabrics, such as Twaron. The heated coating is sprayed on using an atmospheric plasma spray torch and is cooled at the point of contact with the fabric to prevent fiber damage. The layer is 50 to 100 μm thick with individual particles sizes of 10-22 μm. The coatings from the particles to the adhesive materials have a high density. This may give a more flexible and lightweight solution than the common ceramic reinforced body armor, but the weight is still relatively high. Other coatings have been explored using a shear thickening fluid, commonly known as a dilatant fluid, which is impregnated into woven aramid fabrics. The rheology of the non-Newtonian fluid behavior has been studied by Raghavan *et al.* [3, 4], Maranzano *et al.* [5] and Lee *et al.* [6]. These works discuss the effects of fluid viscosity increase when the applied shear rate is increased. The increase in fluid viscosity is key to energy dissipation of impacts (i.e. ballistic). The above works investigate coatings and infusions to dissipate impact energy. More works of Lee *et al.* [7, 8], Wetzel *et al.* [9], Egres *et al.* [10, 11], and Tan *et al.* [12] studied the performance of the silica infused fabrics. The first three author groups consider a centrifugation and exchange process of micron size silica suspended in water and adds polyethylene glycol (PEG) which transforms the mixture into Shear Thickening Fluid (STF). In other approaches, PEG is incrementally added to the silica suspension;

and water is removed through evaporation. The process is repeated until the mixture reaches the desired ratio of silica to PEG by weight. STF developed in this manner is dissolved in ethanol, impregnated into Kevlar fabric, and then dried to remove ethanol. The resulting composite is Kevlar impregnated with a mixture of PEG and silica. These studies report the ballistic performance of composite materials composed of Kevlar fabric impregnated with a colloidal STF. The impregnated Kevlar fabric yields a flexible, yet penetration resistant composite material. Measurements have demonstrated a significant improvement in ballistic and stab penetration resistance due to the addition of STF to the fabric without any loss in material flexibility. Such enhancement in performance has been attributed to the increase in the yarn pullout force upon transition of the STF to its rigid state during impact. Furthermore, STF impregnated Kevlar has superior stab resistance, in addition to flexible ballistic protection. While these preliminary studies establish the viability of the STF-fabric composite as a future flexible body armor system, the entire scope of particle-polymer interaction along with the complexities associated with fabric impregnation must still be addressed before an optimal, lightweight STF-fabric system can be developed.

The current work involves the basic constituents of STF, but the fabrication of the STF is not undertaken and the idea of the impact resistance is due to the silica particles themselves rather than the shear thickening effects since the fluid mixture is dried out after fabric impregnation. In further attempts to enhance the penetration resistance, nanotechnology is incorporated by the use nanoscale particles rather than commonly used micron size particles. Because of the greater surface area with nanoparticles, the surface energy will be higher to improve bonding between the fiber and matrix [13-15]. The benefits of nanoparticle infusion come from the increase in influence zones, which introduces a perturbed layer where the properties are different than that of the particle and that of the polymer [16]. Ultrasonic cavitation is used, over other mixing techniques, to accelerate and intensify diffusion, dissolution, dispersion and emulsification [13] of the silica nanoparticles into the liquid medium. This causes modifications of the particle ($SiO_2$) surfaces [17] that enhance their interaction with the polymer (PEG) at the interface [18-20]. In nanocomposites these interface zones serve as catalysts for prolific crack growth, creating a greater amount of new surfaces than would otherwise be the case [21-23]. The creation of new surfaces can serve as an efficient mechanism to dissipate kinetic energy in the event of an impact.

In addition to nanoparticle infusion, the chemical and bonding of the nanoparticles is further enhanced by functionalization. This increases the number of bond sites on the particles to further strengthen the bonding with the surrounding matrix.

In view of the discussion, it is concluded that a system of functionalized $SiO_2$ nanoparticles dispersed ultrasonically into PEG and then impregnated with Kevlar fabric constitute a materials system which should be equivalent to or better than the currently used STF-fabric composites for flexible body armor protection.

Materials synthesis, test methodology, results, and theoretical analysis is presented.

## 2 Functionalization of Silica Nanoparticles

In an attempt to further improve the penetration resistances of the composite, silica particles were functionalized with a silane coupling agent. Such functionalization was first tested with extruded Nylon 6 filaments in another research project. This resulted in a 55% and 75% gain in Young's Modulus and the Tensile Strength, respectively, of the filaments [14], [24]. The terms silated, functionalized and modified particles will be used through out the text. The three terms are interchangeable and refer to the addition of the silane coupling agent to the surface of the particles. Organosilane used in this investigation was procured from Gelest [25].

Silane coupling agent is used to form durable bonds between inorganic and organic materials, such as the silica nanoparticles and PEG, where silane is extremely effective with silica [25].

The inorganic compatibility comes from the alkoxy groups (X) attached to the silicon atom in the Silane's molecular structure, shown in Fig. 1. This bond is hydrolytically unstable and in the presence of moisture hydrolyses to an intermediate Si-OH bond. Then it condenses with the surface bound OH groups on the inorganic surface (i.e. silica nanoparticles) to form stable bonds. The organofunctional group remains available for covalent reaction or physical interaction with other phases such as, in the present case, PEG.

## 3 Materials and Synthesis

### 3.1 Unmodified Particle Infusion

Actual fabrication procedures include the silica nanoparticles dispersed, by sonication, directly into a mixture of PEG and ethanol at a ratio of 7.9:6.5:85.6 (SiO2:PEG:Ethanol) by weight. This ratio eventually resulted in a mixture of silica and PEG at 55:45 by weight after drying out ethanol. The addition of ethanol aides in the dispersion, during sonication, to breakup the silica agglomerations and to aide the infusion of the silica-PEG mixture into the Kevlar fabric. After sonication for about an hour, the mixture was used to soak 12 layers of Kevlar fabric cut in dimensions of 30.48 cm x 38.10 cm. To impregnate the fabric, the layers were placed in a sealed plastic bag along with the sonicated mixture. After, approximately fifteen minutes, each individual fabric layer was laid flat in the furnace and baked at 75°C until they were dry, i.e. all the ethanol had evaporated. The 12 layers of Kevlar impregnated with the silica-PEG mixture resulted in an areal density of approximately 0.250 g/cm2. This fabrication procedure completely bypassed the heating and centrifugation of the mixture and the addition of ethanol prior to soaking as compared to the fabrication of STF.

### 3.2 Modified Particle Infusion

The modification of the silica nanoparticles with the use of silane is followed according to the manufacturer's procedures and is derived from the surface area of the nanoparticles. Based on the fact that one gram of silane covers a surface area of 358 $m^2$, silane was added to a 95% ethanol – 5% water mixture to yield a 2% final concentration of silane. The actual amount of each chemical used is listed in Table 1. Five minutes was allowed for hydrolysis and silanol formation and then stirred for 2 minutes. The silica nanoparticles were silated by stirring them in the solution for 2-3 minutes. The mixture was placed in a furnace at 110°C until dry. Normal synthesis with the modified particles is continued as discussed in the previous section.

Table 1: The amount of ethanol, water and silane used to functionalize 5.5 grams of 7 nm and 30 nm silica particles according the manufacturers procedures.

| Particle Size (nm) | Specific Surface Area ( $m^2/g$) | Ethanol (grams) | Water (grams) | Silane (grams) |
|---|---|---|---|---|
| 7 | 390.0 | 285 | 15 | 6 |
| 30 | 90.9 | 66.5 | 3.5 | 1.4 |

## 4 Testing

### 4.1 FTIR Analysis

It is observed, in Fig. 2, that the modified silica nanoparticles absorb more energy than the silica particles without silane. The largest peak wavenumber near 1090 cm-1, represents the siloxane bond (Si-O-Si) which naturally occurs in silica. The infrared (IR) absorption of the siloxane bond increased from approximately 0.2 to over 1.0 with the addition of silane modification of the silica nanoparticles, indicating an increase in the number of chemical bonding.

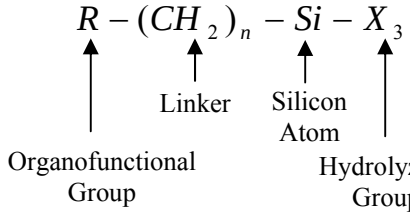


Fig. 1: Molecular structure of the trialkoxysilane coupling agent

The peak is sharper signifying a stronger siloxane bond. An increase in area under the curve suggests an increase in the concentration of Si-O-Si bonds due to functionalization. At approximately 800 $cm^{-1}$, there is another spike that has increased due to the modification of the silica particles. This enhanced peak, up to 35% absorbance, indicates formation of a new carbon-hydrogen (C-H) single bond because of surface modification of the silica particles. The presence of other high frequency bonds, such as methyl ($CH_3$) group and the methylene ($CH_2$) group arising from the silane linker is apparent at approximately 2900 $cm^{-1}$.

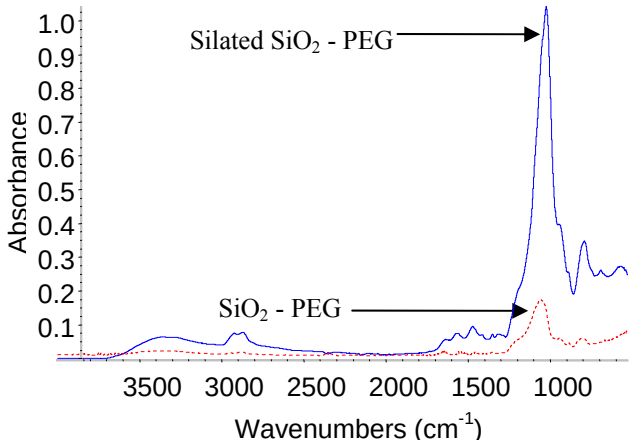


Fig. 2. FTIR results of modified (silated) and unmodified 7nm silica particles.

## 4.2 Drop Tower Tests

Kevlar composites were fabricated using the above procedures, and were tested using a drop tower constructed based on National Institute of Justice Standard 0115.0 (NIJ115). Basically, the setup consists of the flexible fabric composite, as the target, laid on top of the NIJ115 backing material and a nylon drop mass with the NIJ115 engineered spike is dropped vertically to strike the target. The drop heights ranged from approximately 0.05 m to 1.0 m to produce theoretical impact energies from 1 J to 17 J with an increment of 1 J. The velocities just prior to impact are measured through a laser speed trap. Using the measured impact velocity, the total mass of the spike and drop mass; the actual impact energy was calculated. Along with the impact energy, the penetration depth is also a factor in classifying stab resistant body armor. The penetration depth was measured by damaged witness papers placed immediately underneath the fabric specimen and underneath consecutive sponge layers that compose the backing material shown in Fig 3.

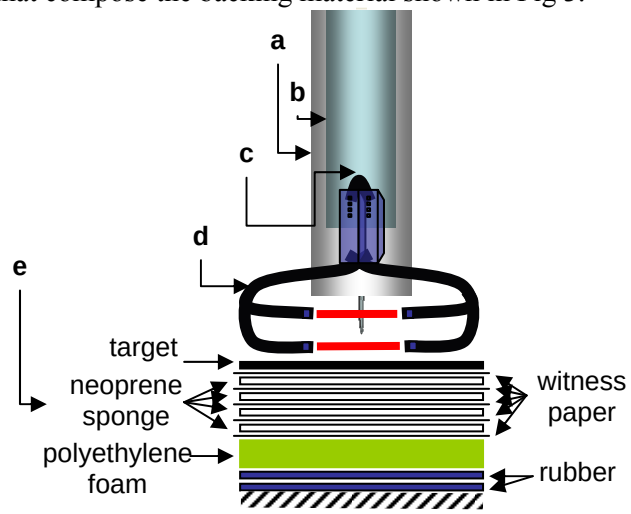


Fig 3. NIJ115 drop tower and system setup; (a) drop apparatus (b) drop mass (c) threat weapon (Spike) (d) velocity measurement zone (e) backing material.

The measurement starts with zero, indicating no penetration beneath the fabric composite, and increases by increments of one to indicate further depth of penetration up to the fifth witness layer.

## 4.3 NIJ Test Results

The impact energies were normalized by dividing by the areal density of the respective fabric composite as listed in Table 2; and these were plotted against the penetration depth, as seen in Fig 4. While the PEG impregnated Kevlar does show improvement relative to the neat Kevlar, the addition of silica nanoparticles is significant in stab resistance. The results show that although the STF fabrication route was bypassed, the sonicated mixture of nanophased silica particles and PEG can impart stab resistance properties to neat Kevlar fabric. The modified 7 nm silica particles and the unmodified 30 nm silica particles at low impact energies show superior stab resistance, allowing no penetration, but allow penetration up to the fourth witness layer at the highest impact energy. The highest depth of penetration for the 7 nm sonicated Silica-PEG and the modified 30 nm sonicated silica-PEG impregnated Kevlar composite is four times less than that of the neat Kevlar. Even the simplest fabrication route of the untreated 7 nm fabric composite exceeded the STF-Kevlar composite above 17.65 J/g/cm$^2$ (4.73 Joules), since it retained its impact resistance up to one layer at the highest impact energy. Focusing on the silated 30nm particles, the penetration resistance proves to be superior at low and high impact energies compared to the current results, which was not achieved by the 7nm sized particles or by the STF-Kevlar composite. The addition of increased particle size with functionalization enhanced the Kevlar composite since it resisted penetration up to 28.85 J/g/cm$^2$ (6.96 J) and only one layer of penetration at higher impact energies up to 70.89 J/g/cm$^2$ (17.01 J) (the maximum capacity of the drop tower).

Table 2: Stab test targets

| Fabric | Nanoparticle Mixture wt% | Single layer areal density (g/cm$^2$) | Number of layers | Target areal density (g/cm$^2$) |
|---|---|---|---|---|
| Neat Kevlar | 0 | 0.018 | 15 | 0.270 |
| PEG Kevlar | 0 | 0.021 | 12 | 0.250 |
| 7 nm Silica-PEG-Kevlar | 15.7 | 0.021 | 12 | 0.250 |
| Silated 7 nm Silica-PEG-Kevlar | 14.4 | 0.021 | 12 | 0.247 |
| 30 nm Silica-PEG-Kevlar | 7.9 | 0.019 | 12 | 0.233 |
| Silated 30 nm Silica-PEG-Kevlar | 11.6 | 0.020 | 12 | 0.241 |
| STF-Kevlar | 25.1 | 0.023 | 12 | 0.271 |

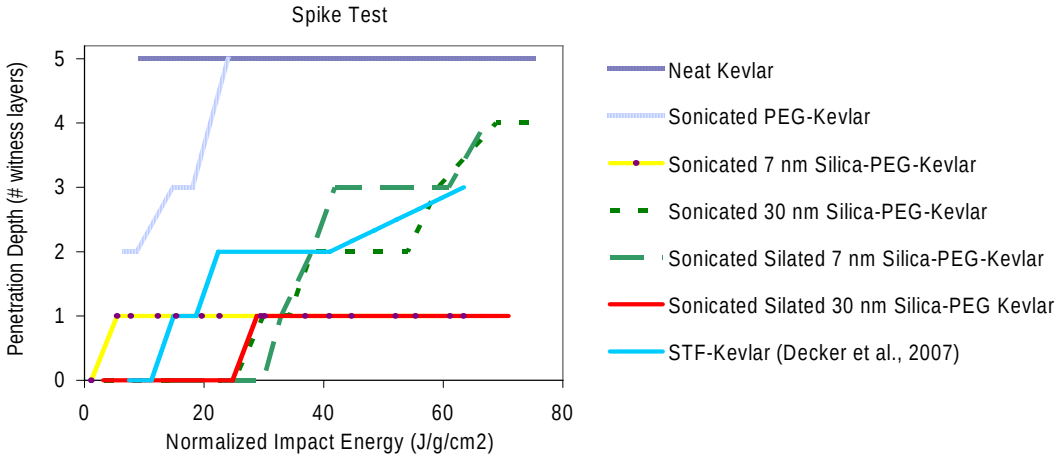


Fig 4. Spike impact results for Neat Kevlar compared to sonicated Silica-PEG mixtures impregnated Kevlar composites normalized with their respective areal densities.

## 5 Microstructures

The improved performance of the Kevlar composite is attributed to the infusion of the silica and PEG mixture coating the fabric. The distribution over the fabric as well as covering the surface area of the tows can only be seen by viewing it at a microscopic level. In addition to the distribution of the mixture infusion, it is important to see the agglomerations that are expected to occur with dispersing the silica nanoparticles into the PEG and Ethanol. Although the clusters will occur naturally, the objective is to still maintain a size in the nanometer range.

### 5.1 Unmodified 7 nm Silica Nanoparticles

A thin coating of silica-PEG mixture formed over the surface of the Kevlar fabric is shown in Fig. 5. This coating is present at the top and bottom of the fabric encompassing the entire area of the laminate. This coating offers the first line of resistance during the spike penetration. The coating consists of agglomerated silica particles embedded in the body of the matrix as seen in Fig. 6.

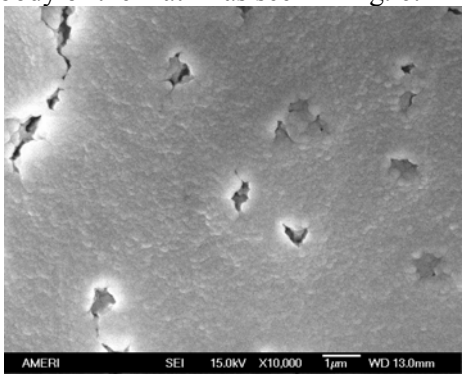


Fig. 5. A thin coating of the silica-PEG mixture on the surface of the Kevlar fabric

The diameter of the agglomerated particles are around 100-150 nm as shown below. These relatively large size particles formed due to the agglomeration of 7nm silica particles in the presence of PEG. Because of the high concentration (55%) of the silica particles, they could not be dispersed fully within the matrix. Nevertheless, the agglomerated particles are still in the nanometer range. Once this thin layer is penetrated, subsequent resistances are offered by the fiber tows impregnated with the particles and the PEG. A number of such tows are shown in Fig 7. Here, a large number of agglomerated particles are adhered to the fiber tows especially in the region where they are bonded with the neighboring tows. The presence of the particles at this inter-tows area also offers resistance should the spike penetrate through this region by contacting the agglomerated silica particles instead of a vacant space. Therefore, it is observed that the mixture of silica-PEG incorporates multiple phases of resistance on to the Kevlar fabric.

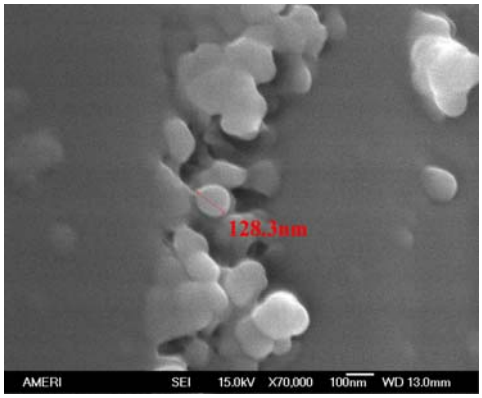


Fig. 6. Agglomerated $SiO_2$ particles and PEG mixture.

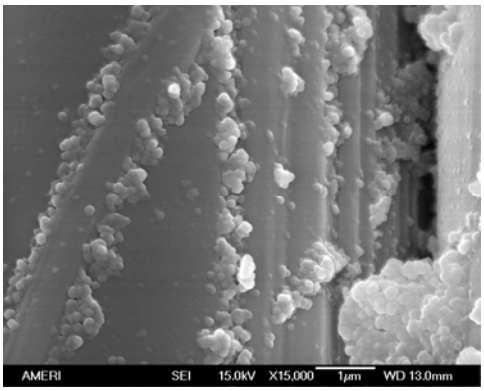


Fig 7. The silica-PEG mixture adhering to the surface of the Kevlar tows.

## 5.2 Functionalized 7 nm Silica Nanoparticles

Fig. 8 shows agglomerated 7 nm particles in the coating over the Kevlar fabric. The modified silica particles mixed with PEG result in agglomerations ranging from approximately 50 to 100 micrometers.

Fig 9, shows an example where a predominant cake-like coating has been dislodged from the Kevlar surface. However, there is still consistent coating on the surface of the tows and between adjacent tows. This adhesion to tows is credited to the silane coupling agent that was used to modify the silica particles and as a result, adhesion continues even after a fiber has been impacted from the spike during the test, seen in Fig. 10.

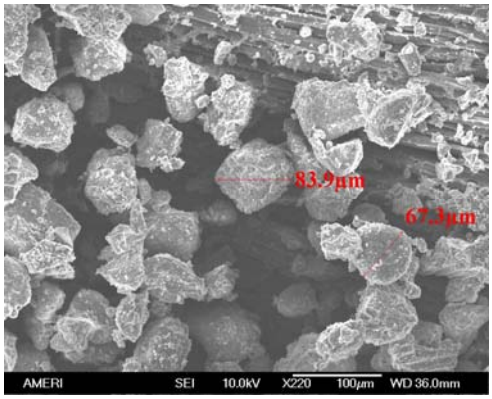


Fig. 8. Agglomerated modified $SiO_2$ particles and PEG mixture on the surface of the Kevlar fabric.

It is projected that the loss of impact resistance at higher impact energies was due to the larger agglomerations, where size of majority of particles was beyond the nanoscale range in the mixture that coat the Kevlar fabric. This reduces the surface energy, in turn reducing particle reactivity with the polymer (PEG) and adherence to the fabric.

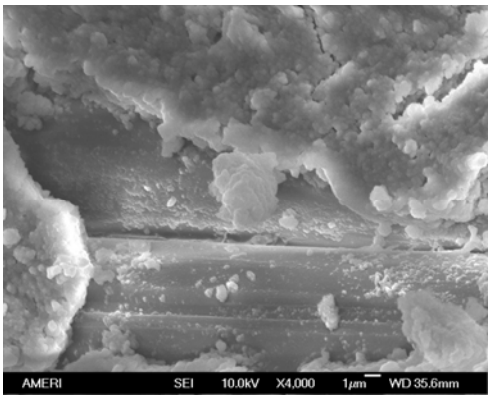


Fig 9. Particle adhesion to the tows of the Kevlar fabric.

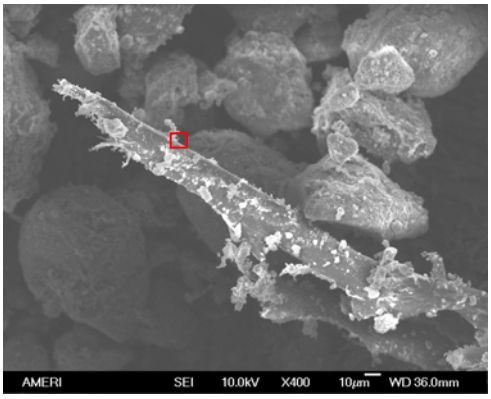


Fig. 10a. Adhesion present after impact on a fractured fiber

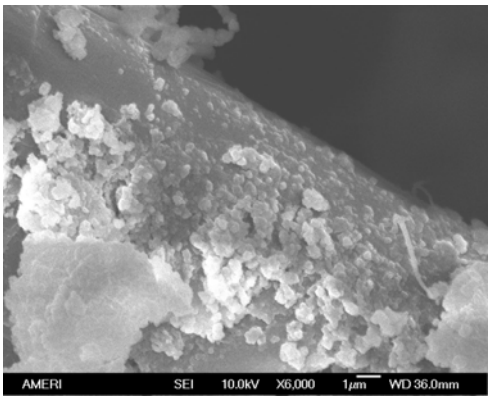


Fig. 10b. A close-up of the particle adhesion retained on the fractured fiber, which reveals particle agglomerates under a micron.

### 5.3 Unmodified 30 nm Silica Nanoparticles

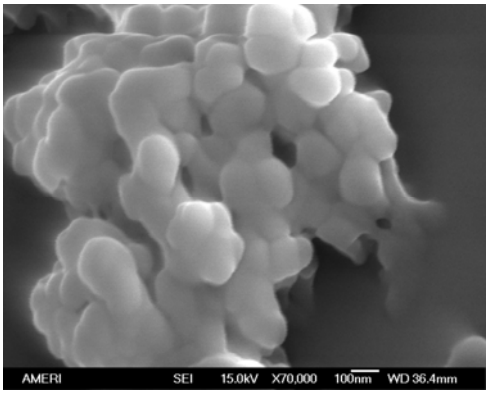


Fig. 11. Agglomerations of the 30 nm silica and PEG mixture on the Kevlar fiber with a size range of approximately 100 nm to 150 nm.

As mentioned previously, differences in particle size were investigated to optimize dispersion and to reduce the agglomerations found in the SEM results of the 7nm particles. To do this, particle diameter was increased from 7nm to 30nm. The microstructure of the 30nm particle mixture impregnated into the Kevlar fabric is shown in Fig. 11.

### 5.4 Functionalized 30 nm Silica Nanoparticles

The 30 nm silated silica-PEG mixture encompassed the entire Kevlar® fiber as seen in Fig. 12. There is a concentration of silica between the fibers, which was seen in Fig 7, in addition to connecting neighboring fibers and dispersed over the regions of the fibers away from the interstitial spaces. Compared to the previous three fabric composites, this is the best coating of the fibers, which enhances the multiple phases of impact resistance.

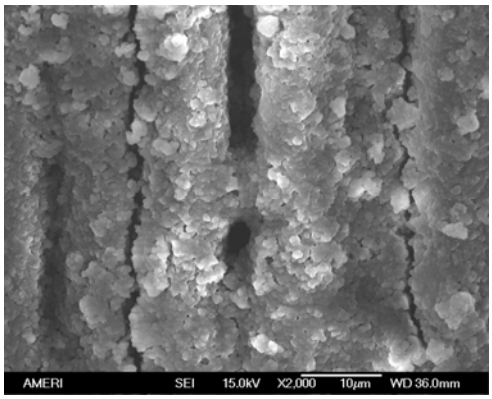


Fig. 12. Adhesion of the modified 30nm silica and PEG coating over the Kevlar® tows and between adjacent tows.

## 6 Depth of Penetration – A Theoretical Analysis

In an attempt to predict the performance of the target material (PEG-$SiO_2$-Kevlar composites) under the dynamic impact of the spike, a theoretical approach was undertaken. In the event of a spike impacting the target at a low velocity, the following scenarios may occur:

1. During a fall, the spike will hit the outermost layer consisting of PEG and silica. Silica particles held together by PEG, forming the cake-like layer will offer the first line of resistance.
2. In the next stage, there is a chance that the spike will hit the Kevlar fabric directly, or at the interstitial spaces between the filaments to offer 2nd and 3rd line of resistances
   - If Kevlar is hit, the radial spoke-like distributed aromatic rings will offer resistance
   - If the spike falls in-between the filaments, there is contact with the silica-PEG mixture to offer resistance
3. As the spike continues to penetrate, it will encounter similar resistances from the subsequent layers.

The above penetration scenarios are depicted in Fig. 13.

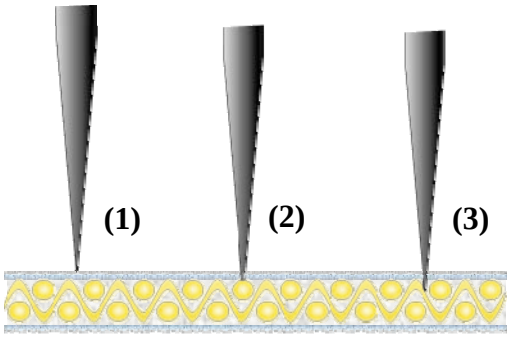


Fig. 13. Schematic of spike penetration scenario for a single ply of the silica-PEG-Kevlar fabric composite.

The modeling of the above penetration phenomena begins by acquiring the load-versus-penetration depth curve through quasi-static penetration of the target, as seen in Fig. 14. A one-dimensional model is developed by assuming that load-deflection behavior at quasi-static loading will be identical under dynamic conditions. Similar assumptions have been undertaken previously [26, 27].

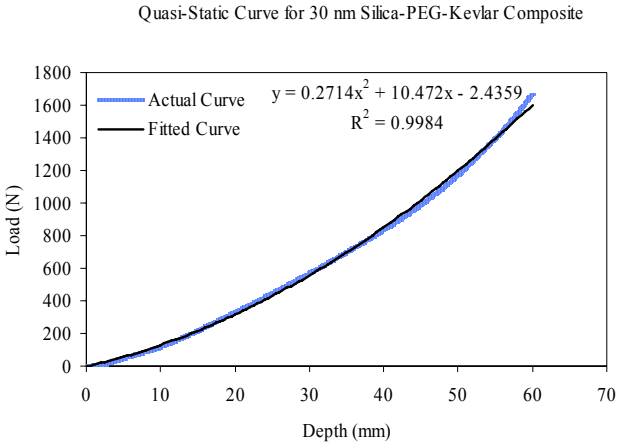


Fig. 14. Quasi-static curve of the 30 nm silica-PEG-Kevlar composite penetrated at a rate of 5mm/min. A curve fitting to the second degree gives a coefficient of determination, $R^2$, of 0.9984.

During impact the motion, *d(t)*, of the spike as it penetrates the target is described using the Newton's 2nd law of motion:

$$m\ddot{d} + P = 0 \qquad (1)$$

Where *m* is the mass of the spike and *P* is the load. During penetration, the velocity of the spike decreases as the kinetic energy is converted to the energy associated with the deformation of the target. The second degree polynomial that best fits the Load-displacement curve in Fig. 14 is:

$$P = C_1 d^2 + C_2 d + C_3 \qquad (2)$$

Where $C_1$ = 271400 Pa, $C_2$ = 10472 N/m and $C_3$ = -2.436 N. The equation of motion is therefore,

$$m\ddot{d} + C_1 d^2 + C_2 d + C_3 = 0 \quad t \geq 0 \qquad (3)$$

Or in terms of *d(t)*

$$\ddot{d} = -\frac{C_1}{m} d^2 - \frac{C_2}{m} d - \frac{C_3}{m} \qquad (4)$$

Assuming a Taylor series expansion of *d(t)*:

$$d(t) = a_0 + a_1 t + a_2 t^2 + a_3 t^3 + a_4 t^4 + \cdots \qquad (5)$$

Where $a_n = \frac{d^{(n)}(0)}{n!}$ and $d^{(n)}$ is the nth derivative of *d(t)* and using the initial conditions of *d(0)=0* and $\dot{d}(0) = V_0$, the Taylor series coefficients in (5) result in,

$$a_0 = \frac{d^{(0)}(0)}{0!} = 0 \text{ and } a_1 = \frac{d^{(1)}(0)}{1!} = V_0$$

From (4),

$$a_2 = \frac{d^{(2)}(0)}{2!} = -\frac{C_3}{2m}$$

Differentiating (4) once gives,

$$d^{(3)} = -\frac{2C_1}{m} d\dot{d} - \frac{C_2}{m}$$

$$\text{i.e.} \quad a_3 = \frac{d^{(3)}(0)}{3!} = -\frac{C_2 V_0}{6m}$$

and differentiating again,

$$d^{(4)} = -\frac{2C_1}{m}\left[\dot{d}^2 + d \cdot \ddot{d}\right] - \frac{C_2}{m}\ddot{d}$$

$$\text{i.e.} \quad a_4 = \frac{d^{(4)}(0)}{4!} = \frac{1}{24}\left[\frac{C_2 C_3}{m^2} - \frac{2C_1 V_0^2}{m}\right]$$

Therefore from (5),

$$d(t) = V_0 t - \frac{C_3}{2m} t^2 - \frac{C_2 V_0}{6m} t^3 + \frac{1}{24}\left[\frac{C_2 C_3}{m^2} - \frac{2C_1 V_0^2}{m}\right] t^4 + \cdots \qquad (6)$$

Finding the first derivative, squaring it, and truncating higher order terms,

$$\dot{d}^2(t) = V_0^2 - \frac{2C_3 V_0}{m} t + \left[\frac{C_3^2}{m^2} - \frac{C_2 V_0^2}{m}\right] t^2 + \left[\frac{4C_2 C_3 V_0}{3m^2} - \frac{2C_1 V_0^3}{3m}\right] t^3 \qquad (7)$$

Letting $t = \frac{d}{V_0}$ in (7), multiplying by ½ *m* and rearranging the terms give the instantaneous energy expression:

$$\tfrac{1}{2} m\dot{d}^2 - \tfrac{1}{2} m V_0^2 = \left(\frac{2C_2 C_3}{3mV_0^2} - \frac{C_1}{3}\right) d^3 + \left(\frac{C_3^2}{2mV_0^2} - \frac{C_2}{2}\right) d^2 - C_3 d \qquad (8)$$

At the maximum depth of penetration, $d_{max}$, $\dot{d} = 0$

$$\left(\frac{2C_2 C_3}{3mV_0^2} - \frac{C_1}{3}\right) d_{max}^3 + \left(\frac{C_3^2}{2mV_0^2} - \frac{C_2}{2}\right) d_{max}^2 - C_3 d_{max} + \tfrac{1}{2} m V_0^2 = 0 \qquad (9)$$

This cubic equation can be solved using Newton-Ramphson method to find $d_{max}$ at any given velocity, $V_0$.

## 6.1 Results

The theoretical data is produced by substituting a range of velocities from 0.1m/s to 4 m/s into (9). Solving for *d* at each velocity gives the theoretical data in Fig. 15. Since the quasi-static test measured the deformation in addition to the depth of penetration to give the equation of motion, the same must be applied to the NIJ stab test. The experimental data for the NIJ stab test of the silica-PEG-Kevlar composite was taken from the results in Fig 4. The same NIJ stab test was run again and a clay material was placed beneath the target to measure the deformation of the backing material. This technique is similar to what is employed in ballistics. It was observed that the back-face

deformation varied with increasing impact velocities. With the increase in impact velocity the back-face deformation in fact decreased. A weighted average technique was then employed to calculate the back-face deformation, and added to the experimental depth of penetration measured earlier.

For the experimental data there are four points because the depth of penetration is measured by the damaged witness layers. For the composite selected, there were only a maximum of four witness layers penetrated which results in four data points. The error between the theoretical and experimental data at the maximum impact velocity of approximately 4 m/s is 78.9% with a difference in displacement of 24.8 mm.

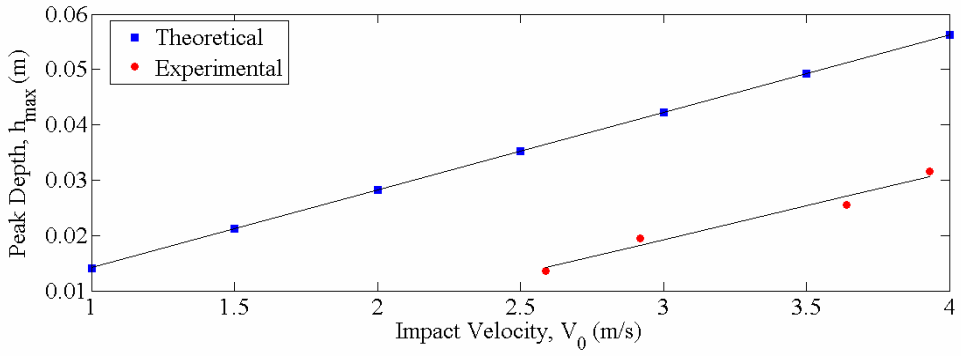


Fig. 15. Peak depth versus impact velocity of the theoretical and experimental data.

## 6.2 Discussion

Although the percent error of the displacement is high the slopes of the two lines are similar with a percent error of 14.85%. The data is offset from one another, but showing a similar trend. The offset between the theoretical and the experimental data is due to the fact that the back-face deformation was not measured with sufficient accuracy using the clay backing. In addition, this difference is expected since the deformation of the backing material is a function of time. During the NIJ stab test, which is a dynamic test, there is less time to deform due to the sudden impact. In the case of quasi-static testing, the force is applied over a 12 minute period of time. During this time the backing material absorbs the energy and in turn, deforms. The actual depth of penetration after quasi-static loading up to 1600 N was only 3.678 mm. This is a total depth of penetration, which includes the thickness of the composite (3.000 mm), the single witness layer (0.178 mm), and the spike protruding past the witness layer by 0.500 mm. The other 55.322 mm (of the 60 mm) was the deformation of the backing material. Also looking at Fig. 14 there are no major peaks or drop offs to designate a sudden penetration, which indicates that the spike under quasi-static loading is slowly and continuously penetrating the composite while deforming the backing material.

It is shown in Fig. 16, that the work done on the target and the backing material exceeds 16 J (the maximum impact energy of the NIJ Stab test results). Initially, the target experienced the quasi-static load and was inspected after 16 J. There was no penetration beneath the back-face of the target. This was not the case for the NIJ Stab test results (Fig 4). The spike penetrated to the fourth witness layer. Not until the work exceeded 38 J with a displacement of 60 mm during quasi-static testing did the spike penetrate through the first witness layer.

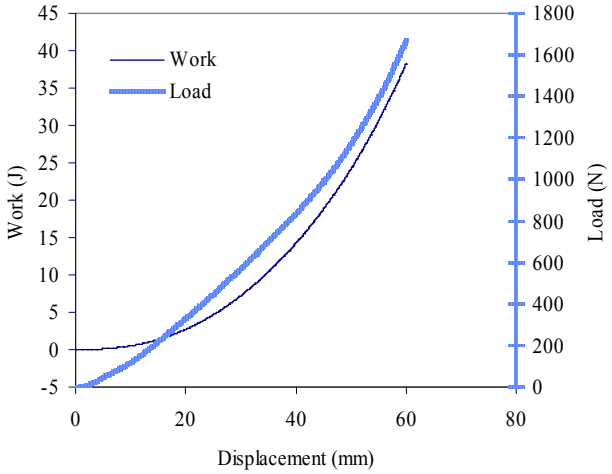


Fig. 16. The work required to displace the spike during quasi-static testing.

## 7 Summary

It has been demonstrated that flexible fabric composite can be developed by ultrasonically dispersing nanoscale silica particles into a mixture

of PEG and ethanol and bypassing the STF fabrication route. It was also shown that the performance of the newly developed nanoparticle-based composites is superior to that of the conventional STF-based composites.

A technique has been established to functionalize nanoscale silica particles and utilize them in the fabrication of the flexible fabric composite. Stab resistance of the composite with functionalized silica particles exceeds any of the present systems. The functionalized system does not allow any penetration up to 5-6 J and only one layer penetration throughout the loading range; i.e., up to 17 J. SEM and FTIR studies have shown that the key to the enhancement in stab resistance is due to the nanoscale dimension of the particle/agglomerate and increase in bonding strength between silica and PEG due to functionalization.

Preliminary work for a theoretical description of the phenomena that transpire during spike penetration through the newly developed composite is suggested based on Newton's 2nd law. Initial calculations were performed, and it is shown that although the prediction of maximum depth of penetration is not accurate, it can capture the trend of the experimental values.

## References


[1] S.S. Deshmukh and G.H. McKinley. Magnetorheological suspensions: Rheology and applications in controllable energy absorption. *Proceedings of the Society of Rheology, October 2003.*

[2] R. Gadow and K. von Niessen. "Lightweight Ballistic with Additional Stab Protection Made of Thermally Sprayed Ceramic and Cermet Coatings on Aramide Fabrics." *Journal of Applied Ceramic Technology* 3, no. 4: 284-292, 2006.

[3] S.R. Raghavan and S.A. Khan. "Shear-induced microstructural changes in flocculated suspensions of fumed silica," *Journal of Rheology* 39, no. 6: 1311-1325, 1995.

[4] S.R. Raghavan and S.A. Khan. "Shear-Thickening Response of Fumed Silica Suspensions under Steady and Oscillatory Shear," *Journal of Colloid and Interface Science* 185: 57-67, 1997.

[5] B.J. Maranzano and N.J. Wagner. 2001. "The effects of particle size on reversible shear thickening of concentrated colloidal dispersions," *Journal of Chemical Physics* 114, no. 23: 10514-10527.

[6] Y.S. Lee and N.J. Wagner. 2003. "Dynamic properties of shear thickening colloidal suspensions," *Rheology Acta* 42, no. 3: 199-208.

[7] Y.S. Lee, Wetzel, E.D. and N.J. Wagner. 2003. "The ballistic impact characteristics of Kevlar® woven fabrics impregnated with a colloidal shear thickening fluid," *Journal of Materials Science* 38, no. 13: 2825-2833.

[8] Y.S. Lee, E.D. Wetzel, R.G. Egres Jr., and N.J. Wagner. 2002. Advanced Body Armor Utilizing Shear Thickening Fluids. *Proceedings of the 23rd Army Science Conference, 2002*.

[9] E.D. Wetzel, Y.S. Lee, R.G. Egres, K.M. Kirkwood, J.E. Kirkwood, and N.J. Wagner. 2004. *Proceedings of NUMIFORM, 2004*.

[10] R.G. Egres, Y.S. Lee, J.E. Kirkwood, K.M. Kirkwood, E.D. Wetzel and N.J. Wagner. 2003. *Proceedings of the 14th International Conference on Composite Materials, July 2003.*

[11] R.G. Egres Jr., M.J. Decker, C.J. Halbach, Y.S. Lee, J.E. Kirkwood, K.M. Kirkwood, E.D. Wetzel, N.J. Wagner. 2004. Stab Resistance of Shear Thickening Fluid (STF)-Kevlar Composites for Body Armor Applications. In *Proceedings of the 24th Army Science Conference, Orlando, Florida, November 29-December 2, 2004*.

[12] V.B.C. Tan, T.E. Tay and W.K. Teo. 2005. "Strengthening fabric armour with silica colloidal suspensions," *International Journal of Solids and Structures* 42: 1561-1576.

[13] C. Nathaniel, H. Mahfuz, V. Rangari, A. Ashfaq and S. Jeelani. 2005. "Fabrication and Mechanical Characterization of Carbon/Epoxy Nanocomposites," *Composite Structures* 67: 115-124.

[14] H. Mahfuz, A. Adnan, V.K. Rangari, M.M. Hasan, S. Jeelani, W.J. Wright and S.J. DeTeresa. 2006. "Enhancement of Strength and Stiffness of Nylon 6 Filaments through Carbon Nanotubes Reinforcements," *Applied Physics Letters* 88, no. 1.

[15] R. Rodgers, H. Mahfuz, V. Rangari, N. Chisholm, and S. Jeelani. 2005. "Infusion of Nanoparticle into SC-15 Epoxy; an Investigation of Thermal and Mechanical Response," *Macromolecular Materials & Engineering* 290, no. 5: 423-429.

[16] V.M. Harik and M. Salas, eds. 2003. *Trends in Nanoscale Mechanics: Analysis of Nanostructured Materials and Multi-Scale Modeling*. Dordrecht, The Netherlands: Kluwer Academic Publishers.

[17] M.W. Urban and E.M. Salazar-Rojas. 1988. "Ultrasonic PTC Modification of poly(vinylidene fluoride) Surfaces and Their Characterization," *Macromolecules* 21: 372-378.

[18] Hesheng Xia, Qi Wang, and Guihua Qiu. 2003. "Polymer-Encapsulated Carbon Nanotubes Prepared through Ultrasonically Initiated In Situ Emulsion Polymerization, *Chemistry of Materials* 15, no. 20: 3879-3886

[19] Toshio Sato, Takeyoshi Uchida, Akito Endo, Shinichi Takeuchi, Naimu Kuramochi and Noricmichi Kawashima. 2002. Study on dispersion

and surface modification of diamond powders by ultrasound exposure. In *Proceedings of the IEEE Ultrasonics Symposium* 1: 521-525.

[20] S. Ramesh, Y. Koltypin and A. Gedanken. 1997. "Ultrasound driven aggregation and surface silanol modification in amorphous silica microspheres," *Journal of Materials Research* 12, no. 12: 3271-3277.

[21] R. Birringer and H. Gleiter. 1998. In: R.W. Cahn, Editor, *Advance in Materials Science, Encyclopedia of materials science and engineering*, Volume 1. Pergamon Press, Oxford: 339.

[22] H. Gleiter. 1989. "Nanocrystalline Materials," *Progress in Materials Science* 33: 223-315.

[23] R. Dagani. 1992. "Nanostructural materials promise to advance range of technologies," *Chemical Engineering & News*: 18-24.

[24] H. Mahfuz. 2006. "Functionalized nanoparticles and their influence on the properties of nanocomposites," *Presented at the Annual Review meeting for ONR*, Washington, D.C.

[25] Gelest, "Gelest Silane Coupling Agents: Connecting Across Boundaries," Gelest, Inc., 2006.

[26] A.E. Giannakopoulos and S. Suresh. 1999. "Determination of Elastoplastic Properties by Instrumented Sharp Indentation," *Scripta Materialia* 40, no. 10: 1191-1198.

[27] E.W. Andrews; A.E. Giannakopoulos; E. Plisson, and S. Suresh: 2002. "Analysis of the impact of a sharp indenter," *International Journal of Solids and Structures* 39, no. 2: 281-295.